Hyperfine interaction for holes in quantum dots: $k \cdot p$ model

Paweł Machnikowski,[1] Krzysztof Gawarecki,[1] and Łukasz Cywiński[2]
[1]*Department of Theoretical of Physics, Faculty of Fundamental Problems of Technology, Wrocław University of Science and Technology, 50-370 Wrocław, Poland*
[2]*Institute of Physics, Polish Academy of Sciences, 02-668 Warsaw, Poland*

(Received 25 February 2019; revised manuscript received 1 August 2019; published 21 August 2019)

We formulate the multiband $k \cdot p$ theory of hyperfine interactions for semiconductor nanostructures in the envelope function approximation. We apply this theoretical description to the fluctuations of the longitudinal and transverse Overhauser field experienced by a hole for a range of InGaAs quantum dots of various compositions and geometries. We find that for a wide range of values of d-shell admixture to atomic states forming the top of the valence band, the transverse Overhauser field caused by this admixture is of the same order of magnitude as the longitudinal one, and band mixing adds only a minor correction to this result. In consequence, the $k \cdot p$ results are well reproduced by a simple box model with the effective number of ions determined by the wave-function participation number, as long as the hole is confined in the compositionally uniform volume of the dot, which holds in a wide range of parameters, excluding very flat dots.

DOI: 10.1103/PhysRevB.100.085305

I. INTRODUCTION

Hyperfine coupling between the spin of a hole localized in a self-assembled quantum dot (QD) and the nuclear spins of the atoms of the host materials has been a subject of intense experimental [1–8] and theoretical [6,9,10] investigations in recent years. The original reason for resurgence of interest in this topic was the prospect of using hole spins as qubits with long coherence times [1,2,8,11–14]. This was motivated by the fact that dephasing of electron spins in QDs, being an obstacle to their application as qubits for quantum information processing purposes, is dominated by their hyperfine (hf) interaction with the nuclear spins of the host material [15–20], and the hole-nucleus coupling was expected to be much weaker than the electron-nucleus one [9,10]. Experimental confirmation of this expectation [1–5] opened the way for using hole-spin qubits in applications, such as creation of long-distance entanglement of hole spins [13], in which their enhanced coherence time and good coupling to photons (holding for both holes and electrons in self-assembled QDs [21,22]) was helpful.

The dominating mechanism in the case of electron hf coupling is the contact interaction [15,23]. While for a purely s-shell state this interaction would be isotropic, lowering the local symmetry leads to mixing of atomic shells in the Bloch functions, which results in an anisotropy of the hf coupling due to dipolar coupling to non-s atomic states [24–26], as in the case of electron states in materials such as Si, in which the states at the bottom of conduction bands have appreciable non-s component [26]. On the contrary, the holes have very small contribution of s states in their wave functions, and therefore interact with nuclei only by weaker (approximately by one order of magnitude [9]) and much more subtle dipole couplings, which are sensitive to the details of their atomic (or Bloch) wave functions. For non-s states, anisotropy can be induced by symmetry breaking without shell mixing, by modifying the hybridization of orbitals. In particular, breaking the symmetry on the mesoscopic level by strong confinement in the growth (z-axis) direction, lifts the degeneracy between heavy-hole and light-hole states and leads to strong anisotropy of the hole hf interaction. As a consequence, for purely heavy-hole state, and for Bloch functions at the top of the valence band being built only from atomic p-shell orbitals of the atoms constituting the crystal, the hf interaction should be of Ising character, with the interaction axis parallel to the growth axis [9]. However, similar to the electron case, atomic shell mixing, in particular the finite amplitude of d states at the top of the valence band (i.e., the p-d hybridization), can give rise to transverse couplings. Such couplings appear also in the presence of finite heavy-light–hole mixing [3,9,10].

These general expectations were confirmed by experiments, showing that the Overhauser field exerted by the nuclei on the hole is about an order of magnitude smaller than the one experienced by the electron in the same dot. In [1,2] qualitative results showing that in InGaAs QDs the coupling of holes to the nuclei is much weaker than that of electrons were obtained from analysis of hole-spin initialization by optical pumping, and coherent population trapping experiment, respectively. In [3] photoinduced circular dichroism of an ensemble of QDs was measured and, from its magnetic field dependence, the value of dot ensemble average of *transverse* Overhauser field experienced by the hole spin was estimated to be $\approx$30 times smaller than the field experienced by the electron spin, and theoretical estimates suggested that the longitudinal coupling should be larger by a factor of about 2, implying rather weak anisotropy of the interaction. Direct measurements of relative magnitudes of the Overhauser field experienced by electrons and holes were then described in [4,5], where nuclei in single InGaAs/GaAs and InP/GaInP single QDs, respectively, were dynamically polarized, and the resulting splittings of electron- and hole-spin states were measured. In both experiments the magnitude of the *longitudinal*

hole Overhauser field was ≈ -0.1 of the electron field, in qualitative agreement with theoretical predictions [9]. It is important to note, however, that the anisotropy of the hole hf interaction was quantitatively characterized in experiments concerning the same quantum dot only very recently in [8], where a value of $\sim 1\%$ of the longitudinal one was measured, while the latter was about 10% of the electron hf interaction, in agreement with previous experiments.

Clearly, the existing experiments do not paint a fully consistent picture, and a number of open questions and controversies need to be investigated. While the longitudinal (along the QD growth axis) hole-nuclear interaction qualitatively agreed with theoretical expectations, large discrepancies in strength of transverse hyperfine interactions were reported, with estimated values of transverse coupling ranging from the same order of magnitude [3] to less than 1% of the longitudinal one [8]. The origin of the transverse interactions is also controversial: while initially heavy-light–hole mixing was invoked [3,9,10] to explain its finite value, the presence of finite admixture of d-symmetry states in states forming the top of valence band in relevant III-V materials was suggested to play a significant, or even possibly dominant, role [6]. Such a substantial admixture of atomic d states in the valence band Bloch functions is in qualitative accordance with earlier theoretical results [27–30]. However, as we show in this paper, the admixture of d states used in [6] to explain the relative magnitudes and signs of contributions to the *longitudinal* Overhauser field coming from various atoms implies that the equilibrium fluctuations of the *transverse* Overhauser field should be comparable to those of the longitudinal one, leading to an apparent qualitative contradiction with the results of [8].

It is important to note that with transverse hole hyperfine coupling being much smaller than the longitudinal one (which, in turn, is lower by an order of magnitude than the coupling for an electron), the coherence time of hole spin polarized along the growth axis can be significantly enhanced by application of large transverse magnetic field perpendicular to this axis [8,9]. Understanding of physical origin of the transverse coupling is thus important, as it would possibly allow for design of QDs (by varying composition/shape/strain, etc.) with the best possible hole-spin coherence properties.

The motivation for this work is the observation that interpretation of most experiments related to physics of carrier and nuclear spins in QDs relies on simplified models of carrier envelope wave functions (e.g., assuming the same envelope shapes for holes and electrons) and all the multiband effects (including the degree of heavy-light–hole mixing), and their relation to QD shape. This includes works on carrier spin coherence (which apart from nuclear effects show influence of charge noise coupling to spin via electric-field-dependent g factors [11,14]), creation of dynamic nuclear polarization [4,5], and optical detection (through changes in Overhauser field-induced spin splitting of electron and holes) of nuclear magnetic resonance of different species of nuclei present in the dot [31]. While such experiments were used to obtain new information on structural properties and strain distribution in QDs [31], the simplicity of some of the above-mentioned assumptions casts a certain degree of doubt on the interpretation of measurement results. In light of the above-discussed disagreements between distinct experiments, more careful studies of hole states and the hyperfine coupling for holes are clearly necessary.

The current state of the art in the theoretical modeling of self-assembled semiconductor structures is to use either atomistic methods [32–34] or multiband $k\cdot p$ theories in the envelope function approximation [35,36]. The latter has found a vast range of applications due to its relatively low computational cost and high versatility. It offers reliable information on the wave-function geometry and band mixing and allows one to quantitatively relate the observed spectral features to fine details of the nanosystem morphology and composition. It can be used not only to compute the carrier states and the resulting optical transitions [37], but also to model carrier-phonon couplings [38] and to evaluate the spin-related properties, including g factors [39,40], the effects of spin-orbit coupling [36,41], as well as phonon-induced spin relaxation and dephasing [42,43]. Therefore, in terms of quantitative accuracy, a simple approach to hyperfine interactions lags behind the current standards in the modeling of carrier wave functions in semiconductor nanostructures and is not on a par with the sophistication of experimental techniques used for the measurements of the relevant quantities. It therefore seems useful to develop a theory that would allow one to combine the hyperfine interaction with realistic modeling of wave functions. Such a more general and accurate theory may be useful in systems with compositional inhomogeneity and controllable carrier localization, like double QDs, or with strong in-plane anisotropy, where band mixing is relatively stronger [44].

The goal of this paper is to revisit the problem of calculation of the anisotropic Overhauser field acting on a hole spin while employing a detailed realistic description of carrier states in QDs. We derive a theoretical description of hyperfine coupling for a carrier confined in a self-assembled semiconductor QD based on the multiband wave function obtained from the $k\cdot p$ theory in the envelope function approximation, taking into account d-wave admixture in the valence band states. In this way, we provide a model of the hyperfine interaction compatible with the standard $k\cdot p$ modeling of carrier states, which opens the way toward combining the effects of hyperfine coupling with reliable modeling of other characteristics of the QD system. As an application of the formalism, we calculate the root-mean-square (rms) fluctuations of the longitudinal and transverse Overhauser field in InGaAs/GaAs QDs and compare the contributions to the transverse field fluctuations from band mixing and d-wave admixture to valence band states.

The paper is organized as follows. In Sec. II we derive the general eight-band $k\cdot p$ Hamiltonian for hyperfine interactions. Next, in Sec. III we apply this formalism to the fluctuations of the Overhauser field felt by a hole in a QD. In Sec. IV we discuss the implications that our results have on hole-spin decoherence and the status of experimental controversies concerning hf interaction of holes, and in Sec. V we summarize our findings. Technical derivations are collected in the Appendix.

II. MULTIBAND HYPERFINE HAMILTONIAN

The hyperfine Hamiltonian describes the interaction of the carrier with all the nuclei (labeled by α and located

at $\boldsymbol{R}_\alpha$),

$$H = 3E_{\rm hf}\sum_\alpha \zeta_\alpha \boldsymbol{A}(\boldsymbol{r}-\boldsymbol{R}_\alpha)\cdot\boldsymbol{I}_\alpha/\hbar, \tag{1}$$

where

$$E_{\rm hf} = \frac{2\mu_0}{3\pi}\mu_{\rm B}\mu_{\rm N}a_{\rm B}^{-3} = 0.5253\ \mu{\rm eV},$$

where $\mu_{\rm B}$ and $\mu_{\rm N}$ are Bohr and nuclear magnetons, respectively, $a_{\rm B}$ is the Bohr radius, μ_0 is the vacuum permeability, $\boldsymbol{I}_\alpha$ is the nuclear spin, ζ_α defines the nuclear magnetic moment for a given nucleus via $\boldsymbol{\mu}_\alpha = \zeta_\alpha\mu_{\rm N}\boldsymbol{I}_\alpha$, and

$$\boldsymbol{A}(\boldsymbol{r}) = \frac{a_{\rm B}^3}{4\hbar}\left[\frac{8\pi}{3}\delta(\boldsymbol{r})\boldsymbol{S} + \frac{\boldsymbol{L}}{r^3} + \frac{3(\hat{\boldsymbol{r}}\cdot\boldsymbol{S})\hat{\boldsymbol{r}}-\boldsymbol{S}}{r^3}\right], \tag{2}$$

with $\boldsymbol{L}$ and $\boldsymbol{S}$ denoting the orbital and spin angular momentum of the carrier and $\hat{\boldsymbol{r}} = \boldsymbol{r}/r$. The first term in Eq. (2) is the Fermi contact interaction between the carrier and nuclear spins, the second term describes the coupling of the nuclear spin to the electric current associated with the orbital motion of the carrier, and the last one is the dipole interaction between the nuclear and carrier spins.

Within the envelope function approach to the $k\cdot p$ theory, the wave functions are decomposed into contributions from various bands λ with Γ-point Bloch functions $u_\lambda(\boldsymbol{r}, s)$,

$$\Psi_\nu(\boldsymbol{r}, s) = \sum_\lambda \psi_{\nu,\lambda}(\boldsymbol{r})u_\lambda(\boldsymbol{r}, s), \tag{3}$$

where the envelopes $\psi_{\nu,\lambda}(\boldsymbol{r})$ are assumed to vary slowly in space (as compared to the lattice constant) and s denotes the spin projection. Most commonly, an eight-band model is used [41], explicitly representing two subbands of the conduction band (belonging to the Γ_{6c} representation of the bulk crystal) and six subbands in the valence band (four-dimensional Γ_{8v} and two-dimensional Γ_{7v}), with the coupling to other bands represented by effective terms resulting from perturbation theory. The eight envelope wave functions $\{\psi_{\nu,\lambda}(\boldsymbol{r})\}$ are commonly thought of as an eight-component "pseudospinor." Consequently, the Hamiltonian (or any other operator) in the envelope function $k\cdot p$ theory can be considered an 8×8 array of operators $H_{\lambda'\lambda}$ in the coordinate representation, such that any matrix element of the original Hamiltonian is given by

$$\langle\nu|H|\mu\rangle = \sum_{\lambda'\lambda}\int d^3r\,\psi^*_{\nu,\lambda'}(\boldsymbol{r})H_{\lambda'\lambda}\psi_{\mu,\lambda}(\boldsymbol{r}). \tag{4}$$

The goal of this section is to apply the envelope function approximation [Eq. (3)] to the hyperfine Hamiltonian (1) and to write it in the form consistent with Eq. (4).

Starting from Eq. (2) and using Eq. (3), the matrix elements of A_i are

$$\langle\nu|A_i(\boldsymbol{r}-\boldsymbol{R}_\alpha)|\mu\rangle = \sum_{\lambda'\lambda}\sum_{ss'}\int d^3r\,\psi^*_{\nu,\lambda'}(\boldsymbol{r})u^*_{\lambda'}(\boldsymbol{r}, s') \times A_{i,s's}(\boldsymbol{r}-\boldsymbol{R}_\alpha)\psi_{\mu,\lambda}(\boldsymbol{r})u_\lambda(\boldsymbol{r}, s), \tag{5}$$

where $A_{i,s's}(\boldsymbol{r})$ denotes the matrix elements of $A_i(\boldsymbol{r})$ with respect to spin states. The Bloch functions are decomposed into parts localized around the anion (A) and cation (C), that are assumed to be normalized and nonoverlapping,

$$u_\lambda(\boldsymbol{r}, s) = \sum_{i={\rm A,C}} a_i^{(\lambda)}u_\lambda^{(i)}(\boldsymbol{r}, s),$$

where $a_{\rm A,C}^{(\lambda)}$ are the contributions of the anionic and cationic atomic orbitals to a given band. Next, we split the space into primitive cells, which are further divided into two parts surrounding the anion and the cation. The integration over the whole space is then performed as integration over the surrounding of each ion and summation over all the ions. We use the fact that the envelope varies slowly, so that in the vicinity of each ion it can be approximated by its value at the ion position $\boldsymbol{R}$. In this way we transfer Eq. (5) into

$$\langle\nu|A_i(\boldsymbol{r}-\boldsymbol{R}_\alpha)|\mu\rangle = v\sum_{\lambda'\lambda}\sum_{\alpha'}\psi^*_{\nu,\lambda'}(\boldsymbol{R}_{\alpha'})A^{\alpha'\alpha}_{i,\lambda'\lambda}\psi_{\mu,\lambda}(\boldsymbol{R}_{\alpha'}), \tag{6}$$

with

$$A^{\alpha'\alpha}_{i,\lambda'\lambda} = \frac{1}{v}\sum_{ss'}\int_{V_{\alpha'}} d^3r\,u^*_{\lambda'}(\boldsymbol{r}, s')A_{i,s's}(\boldsymbol{r}-\boldsymbol{R}_\alpha)u_\lambda(\boldsymbol{r}, s), \tag{7}$$

where v is the volume of the primitive crystal cell and V_α denotes the volume surrounding the ion α (the arbitrariness in choosing this volume is unimportant in view of the strong localization of Bloch functions around the ions [6]). Since the variation of the envelope functions is slow, the summation in Eq. (6) realizes a coarse-grained integration over the whole space. Thus, Eq. (6) brings matrix elements of the hyperfine Hamiltonian (1) to the form of Eq. (4) with

$$H_{\lambda'\lambda}(\boldsymbol{r}) = 3E_{\rm hf}v\sum_{\alpha'\alpha}\delta(\boldsymbol{r}-\boldsymbol{R}_\alpha)\zeta_\alpha\boldsymbol{A}^{\alpha'\alpha}_{\lambda'\lambda}\cdot\boldsymbol{I}_\alpha/\hbar. \tag{8}$$

In order to evaluate Eq. (7) one needs a model of the Bloch functions. Following [9], we choose to represent them as combinations of normalized hydrogenlike functions $f^{(i)}_{lm}(\boldsymbol{r})$ with definite rotational symmetry ($l = s, p, d$), characterized by the orbital exponents $\xi_{l,\alpha}$ [45,46] that depend on the nuclear species occupying the site α. Thus,

$$u^{(i)}_\lambda(\boldsymbol{r}, s) = \sqrt{v}\sum_{lm}c^{(\lambda s)}_{lm}f^{(i)}_{lm}(\boldsymbol{r}-\boldsymbol{r}_i), \tag{9}$$

where $l = 0, 1, 2$, $m = -l, \ldots, l$. The valence band Bloch functions are composed of p and d atomic orbitals, weighted by the amplitudes α_p and α_d, respectively, with $|\alpha_p|^2 + |\alpha_d|^2 = 1$. We suppress the principal quantum number n since only one orbital of each symmetry is relevant for a given atom. The coefficients $c^{(\lambda s)}_{lm}$ for purely p-band ($l = 1$) states can be found from angular momentum addition and are widely available in the literature related to the $k\cdot p$ method [41,47]. The extension to the d admixture follows immediately from the explicit form of the basis functions of the F_2 representation of the T_d point group, as given in [6].

The matrix element in Eq. (8) has two contributions: the local, or short-range (SR) one, from the surrounding of the ion in question ($\alpha' = \alpha$) and the long-range (LR) one, from all the other ions in the crystal (including the neighboring cations for an anion and vice versa). The LR contribution has been estimated to be negligible [9,10,25,26]. In the following, we only take into account the SR contribution.

The detailed derivation of the SR contributions, which systematically extends the existing theoretical description [3,6,9,24] to multiband wave functions, is given in the Appendix. The resulting matrix elements $A^{\alpha\alpha}_{i,\lambda'\lambda}$ must have appropriate transformation properties, hence, they can be expressed by the standard matrices used to define point-group invariants when constructing the $k\cdot p$ theory. In order to use this convenient notation, we split the array $\{H_{\lambda'\lambda}\}$ into blocks corresponding to the three irreducible representations spanning the eight-band $k\cdot p$ model

$$H = \begin{pmatrix} H_{6c6c} & H_{6c8v} & H_{6c7v} \\ H_{8v6c} & H_{8v8v} & H_{8v7v} \\ H_{7v6c} & H_{7v8v} & H_{7v7v} \end{pmatrix}, \tag{10}$$

with

$$H_{b'b} = H^{\dagger}_{b'b} = E_{\mathrm{hf}}\upsilon \sum_{\alpha} \delta(\boldsymbol{r}-\boldsymbol{R}_{\alpha}) a^{(b')*}_{\alpha} a^{(b)}_{\alpha} \zeta_{\alpha} \xi^{3}_{s,\alpha} \tilde{H}^{(\alpha)}_{b'b} \tag{11}$$

(the index b labels blocks and we assume that $a^{(\lambda)}_{\alpha}$ is the same for all bands λ in a given block b), and find

$$\tilde{H}^{(\alpha)}_{6c6c} = \boldsymbol{\sigma}\cdot\boldsymbol{I}_{\alpha}/\hbar, \tag{12a}$$

$$\tilde{H}^{(\alpha)}_{8v8v} = \left(-\frac{8}{5}\tilde{M}^{(\alpha)}_{p} + \frac{39}{7}\tilde{M}^{(\alpha)}_{d}\right)\boldsymbol{J}\cdot\boldsymbol{I}_{\alpha}/\hbar - \frac{12}{7}\tilde{M}^{(\alpha)}_{d}\boldsymbol{\mathcal{J}}\cdot\boldsymbol{I}_{\alpha}/\hbar, \tag{12b}$$

$$\tilde{H}^{(\alpha)}_{7v7v} = \left(-4\tilde{M}^{(\alpha)}_{p} + \frac{2}{7}\tilde{M}^{(\alpha)}_{d}\right)\boldsymbol{\sigma}\cdot\boldsymbol{I}_{\alpha}/\hbar, \tag{12c}$$

$$\tilde{H}^{(\alpha)}_{6c8v} = -\frac{9}{\sqrt{5}}\tilde{M}^{(\alpha)}_{sd}(T_{xy}I_{\alpha,z} + T_{yz}I_{\alpha,x} + T_{zx}I_{\alpha,y})/\hbar, \tag{12d}$$

$$\tilde{H}^{(\alpha)}_{6c7v} = 0, \tag{12e}$$

$$\tilde{H}^{(\alpha)}_{7v8v} = -\sqrt{3}\left(\tilde{M}^{(\alpha)}_{p} - \frac{15}{7}\tilde{M}^{(\alpha)}_{d}\right)\boldsymbol{T}\cdot\boldsymbol{I}_{\alpha}/\hbar, \tag{12f}$$

where $\tilde{M}^{(\alpha)}_{p,d} = |\alpha^{(\alpha)}_{p,d}|^2 M^{(\alpha)}_{p,d}$, $\tilde{M}^{(\alpha)}_{sd} = \alpha^{(\alpha)}_{d} M^{(\alpha)}_{sd}$, the dimensionless quantities $M_{p,d,sd}$ characterize the geometry of the atomic functions and are explicitly defined in the Appendix, $\boldsymbol{\sigma} = (\sigma_x, \sigma_y, \sigma_z)$ are Pauli matrices, $\boldsymbol{J} = (J_x, J_y, J_z)$ are the matrices of the four-dimensional ($j = \frac{3}{2}$) irreducible representation of angular momentum $\boldsymbol{\mathcal{J}} = (J^3_x, J^3_y, J^3_z)$,

$$T_x = \frac{1}{3\sqrt{2}}\begin{pmatrix} -\sqrt{3} & 0 & 1 & 0 \\ 0 & -1 & 0 & \sqrt{3} \end{pmatrix},$$

$$T_y = \frac{-i}{3\sqrt{2}}\begin{pmatrix} \sqrt{3} & 0 & 1 & 0 \\ 0 & 1 & 0 & \sqrt{3} \end{pmatrix}, \quad T_z = \frac{\sqrt{2}}{3}\begin{pmatrix} 0 & 1 & 0 & 0 \\ 0 & 0 & 1 & 0 \end{pmatrix},$$

and $T_{ij} = T_i J_j + T_j J_i$. Here, the equation for $\tilde{H}_{8v8v}$ reproduces the result of [6].

From Eq. (12b) it is clear that for a purely heavy-hole (hh) state the only flip-flop terms appear as a result of d-shell admixture via the J^3_i terms that reflect the lowered symmetry of the crystal as compared to the full rotation group. As we show in the Appendix, these terms originate from the spin part of the dipole hyperfine coupling [the last term in Eq. (2)]. Interband terms in the Hamiltonian lead also to flip-flop processes induced by band mixing but, as we will see below, this effect is much weaker.

III. HYPERFINE COUPLING FOR THE HEAVY-HOLE GROUND STATE

In this section we apply the general formalism of Sec. II to the ground-state Zeeman doublet of the nominally heavy-hole state in a range of self-assembled QDs with varying size, shape, and composition. We characterize the fluctuations of the Overhauser field felt by the hole that is the key factor determining the hyperfine-induced spin dephasing.

A. QD model and wave functions

The envelope functions for the QD ground state are computed for a few series of QD structures with the eight-band $k\cdot p$ theory. In all the cases the composition of the QD is uniform and corresponds to the stoichiometric formula $In_xGa_{1-x}As$. The QD is placed on a wetting layer of the same composition and thickness equal to the GaAs lattice constant $a = 0.565$ nm.

We account for the strain within continuous-elasticity approach [48]. We take into account the piezoelectric potential, up to the second order in polarization [49]. The magnetic field enters via Peierls substitution within the gauge-invariant scheme, described in detail in [50]. The detailed description of the model as well as parameters used in computations are given in [36].

Recently, the exponents of the atomic basis functions were related to measurable crystal properties [51] via tight-binding calculations. However, the Slater orbitals commonly used in the tight-banding models are inappropriate for calculating the hyperfine effects, as they only capture the asymptotic behavior of the wave functions away from the nucleus, and are all zero (even those representing the s states) at the position of the nucleus. Thus, although the results of [51] show some promise for more accurate modeling of the Bloch functions, for our purpose we still need to find an appropriate parametrization of the wave functions. We do so by requiring consistency with the available experimental and theoretical data: the hole-to-electron ratio of Overhauser fields [6], Ga and As wave functions at the nucleus [52], and d-shell admixture and anion-cation distribution in GaAs [30]. With the scarce quantitative data available, the parametrization remains to a large extent underdetermined. Based on the relations of the Slater exponents [45,46,51], we arbitrarily set the s-shell exponents for In the same as for Ga and assume $\xi_p = 0.85\xi_s$ for all atoms. The d-shell exponents are then determined from the data of [6]. This parametrization is still to a large extent arbitrary, and should be considered a starting point for further improvements as new experimental and computational data become available.

Table I lists the proposed values of the parameters relevant for the modeling of Bloch functions as well as those describing the hyperfine couplings (see Sec. II and Appendix): nuclear spin quantum numbers, ζ coefficients and relative abundances r for the nuclei of interest, the atomic wave-function exponents ξ and the resulting M parameters, as well as the d-state admixture amplitudes $|\alpha_d|^2$ and cation-anion distributions of charge density for the conduction and valence bands ($|a^{(\mathrm{cb})}_{\mathrm{C/A}}|^2$ and $|a^{(\mathrm{vb})}_{\mathrm{C/A}}|^2$, respectively). At the bottom of Table I we list the resulting values of the electron

TABLE I. Nuclear [15] and atomic parameters.

	^{69}Ga	^{71}Ga	^{113}In	^{115}In	^{75}As
I	3/2	3/2	9/2	9/2	3/2
ζ	1.344	1.708	1.227	1.230	0.959
r	0.604	0.396	0.0428	0.9572	1
ξ_s	3.9		3.9		4.4
ξ_p	3.3		3.3		3.7
ξ_d	10.5		8.9		11.9
M_p	0.050		0.050		0.050
M_d	0.33		0.20		0.33
M_{sd}	0.048		0.034		0.049
$\lvert\alpha_d\rvert^2$	0.20		0.50		0.05
$\lvert a^{(\mathrm{cb})}_{\mathrm{C/A}}\rvert^2$	0.50				0.50
$\lvert a^{(\mathrm{vb})}_{\mathrm{C/A}}\rvert^2$	0.35				0.65
$A^{(\mathrm{e})}$ μeV	41.9	53.2	38.2	38.3	42.9

hyperfine coupling constant $A^{(\mathrm{e})} = 2E_{\mathrm{hf}}|a_{\mathrm{C}}|^2\zeta\xi_s^3$ for each atom, which for Ga and As are very close to those determined in [52].

The proposed model is a combination of a standard $k\cdot p$ approach to computing the envelope wave functions, and a model of atomic wave functions that is necessary for the calculation of the hyperfine couplings. Although the latter must be done on the atomistic level, the $k\cdot p$ model itself is not atomistic and remains at the usual mesoscopic level: the strain is treated within a continuous approach, and the standard values of parameters are used, unrelated to the model of Bloch functions used in the second stage. In the $k\cdot p$ calculation, alloying is taken into account in a coarse-grained manner, by interpolating parameters according to the local composition (virtual crystal approximation), while in the hf calculations explicit counting of ions forces us to implement a particular distribution of atoms and isotopes and to average over a few realizations of the alloy disorder.

B. Effective Hamiltonian

We find the effective Hamiltonian describing the hyperfine interactions in the heavy-hole ground state by projecting Eq. (1) onto the two-dimensional space of the ground-state doublet. We denote the eigenstates in the ground-state doublet (as resulting from the $k\cdot p$ diagonalization) by $|\uparrow\rangle$ and $|\downarrow\rangle$ (hence the two basis states are defined with respect to the spin quantization axis) and define operators Σ_i corresponding to Pauli matrices in this two-dimensional subspace $\Sigma_z = |\uparrow\rangle\langle\uparrow| - |\downarrow\rangle\langle\downarrow|$, etc. The Hamiltonian given in Eq. (1) is linear in the nuclear spins, hence, its projection on the two-dimensional subspace can be written as

$$H = \frac{1}{2}\sum_\alpha\sum_{ij}\mathcal{H}^{(\alpha)}_{ij}(I_{\alpha,i}/\hbar)\Sigma_j, \tag{13}$$

where

$$\mathcal{H}^{(\alpha)}_{ij} = 3E_{\mathrm{hf}}\zeta_\alpha\xi^3_{s,\alpha}\,\mathrm{Tr}[A_i(\boldsymbol{r}-\boldsymbol{R}_\alpha)\Sigma_j].$$

This Hamiltonian has the form of a Zeeman Hamiltonian

$$H = \tfrac{1}{2}\boldsymbol{h}\cdot\boldsymbol{\Sigma},$$

with the quantity $\boldsymbol{h}$, defining the Overhauser field, with components given by

$$h_j = \sum_\alpha\sum_i \mathcal{H}^{(\alpha)}_{ij}I_{\alpha,i}/\hbar.$$

We assume here that the nuclei are in a thermal state without any dynamical polarization. Except for unrealistically low temperatures, this means that the nuclear density matrix is maximally mixed. The mean square of a given component of $\boldsymbol{h}$ is then given by

$$\begin{aligned}\langle h_j^2\rangle &= \sum_{\alpha\alpha'}\sum_{ii'}\mathcal{H}^{(\alpha)}_{ij}\mathcal{H}^{(\alpha')}_{i'j}\langle I_{\alpha,i}I_{\alpha',i'}\rangle/\hbar^2\\ &= \frac{1}{3}\sum_\alpha I_\alpha(I_\alpha+1)\sum_i\left(\mathcal{H}^{(\alpha)}_{ij}\right)^2,\end{aligned}$$

where the last equality assumes that angular momenta of different nuclei as well as different components of nuclear spin are uncorrelated.

In the simplest approximation, one considers a purely heavy-hole wave function which occupies a region of uniform composition and is the same for both spin orientations. Then, by direct inspection of Eq. (12b) one finds

$$\begin{aligned}\mathcal{H}^{(\alpha)}_{ii} &= 2vE_{\mathrm{hf}}|\psi(\boldsymbol{R}_\alpha)|^2\zeta_\alpha\xi^3_{s,\alpha}\mathcal{M}^{(\alpha)}_i,\\ \mathcal{H}^{(\alpha)}_{ij} &= 0, \quad i\neq j\end{aligned}$$

where

$$\begin{aligned}\mathcal{M}^{(\alpha)}_x = \mathcal{M}^{(\alpha)}_y &= \tfrac{9}{7}\tilde{M}^{(\alpha)}_d,\\ \mathcal{M}^{(\alpha)}_z &= \tfrac{12}{5}\tilde{M}^{(\alpha)}_p - \tfrac{18}{7}\tilde{M}^{(\alpha)}_d.\end{aligned}$$

Since $M^{(\alpha)}_i$ depends only on the species of the ion α and $\psi(\boldsymbol{R})$ changes slowly, one can write for the ternary compound $\mathrm{In}_x\mathrm{Ga}_{1-x}\mathrm{As}$

$$\langle h_j^2\rangle = 4E_{\mathrm{hf}}^2 v\int d^3R|\psi(\boldsymbol{R})|^4\sum_i\frac{I_i(I_i+1)}{3}q_i\left(\zeta_i\xi^3_{s,i}\mathcal{M}^{(i)}_j\right)^2, \tag{14}$$

where i runs through all the nuclear species, $q_i = (a_{\mathrm{C}}^{(\mathrm{hh})})^4 r_i x$ for In isotopes, $q_i = (a_{\mathrm{C}}^{(\mathrm{hh})})^4 r_i(1-x)$ for Ga isotopes, and $q_i = (a_{\mathrm{A}}^{(\mathrm{hh})})^4$ for As. The quantity

$$N = \left[v\int d^3R|\psi(\boldsymbol{R})|^4\right]^{-1}$$

is the effective number of the primitive cells encompassed by the wave function (the wave-function participation number [53]) which links the presented theory to the *box model* in which the wave function is considered constant, with the value $1/\sqrt{vN}$ over a volume of N unit cells.

The analogous box-model formula for the electron, which can be inferred directly from Eq. (12a), is

$$\langle h_j^2\rangle = 4E_{\mathrm{hf}}^2 v\int d^3R|\psi(\boldsymbol{R})|^4\sum_i\frac{I_i(I_i+1)}{3}q_i\left(\zeta_i\xi^3_{s,i}\right)^2, \tag{15}$$

with $a_{\mathrm{C}}^{(\mathrm{hh})}$ and $a_{\mathrm{A}}^{(\mathrm{hh})}$ in q_i replaced by the conduction band values $a_{\mathrm{C}}^{(\mathrm{e})}$ and $a_{\mathrm{A}}^{(\mathrm{e})}$, respectively.

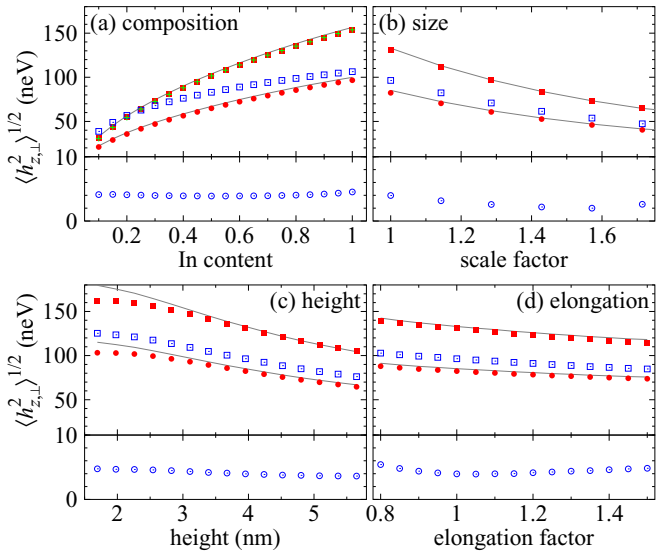

FIG. 1. The dependence of the root-mean-square average of the hole hyperfine field fluctuations for $B = 8$ T in the Faraday geometry as a function of QD composition (a), size (b), height (c), and shape (d). Squares show the fluctuations of the field component along the growth (z) axis while circles represent the fluctuations of the transverse components (averaged over the in-plane directions). Full red symbols correspond to the model with a d-state admixture to the valence band, while the open blue symbols show the values for purely p-type states. The solid gray lines show the box model approximation based on the inverse wave-function participation number, given by Eq. (14). The green crosses in (a) show the results at $B = 0.1$ T. The lower part of the vertical axis has been expanded for clarity.

C. Results and discussion

In this section we study the characteristic strength of the coupling to longitudinal and transverse fluctuations of the Overhauser field felt by a hole in the QD (nominally heavy-hole) ground state. All the results are averages of 10 repetitions in order to account for the random alloying and isotope distribution, resulting in a standard deviation of the numerical result on the order of 1% of the average value.

Figure 1 shows the results for four series of structures with different size and composition. The magnetic field is oriented here in the growth direction (Faraday configuration), hence, the z axis is along the symmetry axis of the structure. In our discussion the notions of "longitudinal" and "transverse" are related to the growth axis. Transverse fluctuations are calculated as the average of fluctuations in two perpendicular directions, $\langle h_\perp^2 \rangle^{1/2} = \langle (h_x^2 + h_y^2))/2 \rangle^{1/2}$.

In Fig. 1(a) we study cylindrically symmetric lens-shaped QDs with base radius $21a = 11.9$ nm and height $h = 7a = 3.96$ nm, and with uniform composition $In_xGa_{1-x}As$, where the indium content x changes from 0.1 to 1. Without d-state admixture to the valence band and without band mixing, a heavy hole couples only to longitudinal hyperfine field. Band mixing induces weak coupling to transverse field (blue open circles), up to a few percent of the longitudinal one. A much stronger coupling, comparable to the longitudinal one, appears as a result of d-state admixture (full red circles). The strong dependence on the In content results from the combination of the large nuclear angular momentum of this element as compared to Ga, and increasing localization in indium-rich QDs (the wave-function participation number N decreases from 52×10^3 to 13×10^3 as x grows from 0.1 to 1). This dependence is much weaker in the case of transverse coupling induced purely by band mixing. The gray solid lines show the results obtained from Eq. (14). In order to relate our multiband numerical wave functions to the simple theory, we define here the wave-function participation number as

$$N' = \left[v \int d^3R \left| \sum_\lambda |\psi_\lambda(\boldsymbol{R})|^2 \right|^2 \right]^{-1}$$

and average the result over the two hh states. The agreement is very good, validating the box model with the wave-function participation number as the effective number of primitive cells. The results for the very weak field of $B = 0.1$ T (green crosses) do not differ considerably from those at $B = 8$ T. This is expected since in a self-assembled QD the in-plane confinement scale ($l_0 \sim 4$ nm) is much smaller than the magnetic length ($l_B \approx 9$ nm at $B = 8$ T) and the resulting relative field-induced correction to confinement ($(l_0/l_B)^4/8$ based on the Fock-Darwin model) is negligible.

Figure 1(b) presents results for a series of QDs with identical compositions $x = 0.75$, starting from the geometry as in the previous case and then uniformly scaling each dimension of the QD up by a factor up to 2 (the data are shown as a function of the linear scaling factor). In Fig. 1(c) the lateral size of the QD is kept fixed as in Fig. 1(a) and the height h is varied. In Fig. 1(d) the QD is made elliptic by relatively elongating the QD shape in plane by a fixed factor along the $(1\bar{1}0)$ crystallographic axis while keeping the height and the size in the other in-plane direction constant [so that *elongation factor* equal to 1 corresponds to the geometry of Fig. 1(a)]. In all these cases the general dependence on the geometry qualitatively follows the prediction of the box model with the effective field fluctuations decreasing with the growing system size. Quantitatively, however, the fluctuations of the Overhauser field only approximately follow the expected scaling as $1/\sqrt{V}$, which is due to the fact that the wave function shrinks slower than the QD when the size of the latter is reduced. In Fig. 1(c) one can see discrepancy between the numerical values and the predictions of the box model for very flat QDs. This results from the leakage of the wave function to the indium-free barrier.

As a reference, in Fig. 2 we show the rms fluctuations of the Overhauser field for an electron in the same structures as in Figs. 1(a) and 1(b). Both the relative anisotropy of the hyperfine coupling, as well as the relative difference between the results with and without d-shell admixture in this case are at most on the order of 10^{-3}, therefore, we show only the results for the z component in the model with the admixture. The values for the electron are five to seven times larger than for the hole, with the electron-to-hole ratio slightly decreasing as the In content grows. The results for the electron are also very well reproduced by the box model using the wave-function participation ratio. As the In content grows from 0.1 to 1, the latter decreases from 119×10^3 (more than twice the value for the hole in the same structure) to 14×10^3 (nearly equal to the hole value).

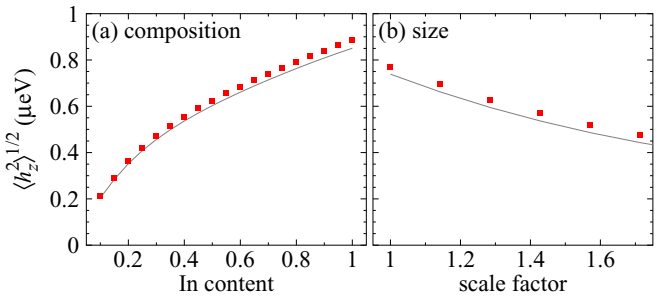

FIG. 2. The dependence of the root-mean-square average of the electron hyperfine field fluctuations for $B = 8$ T in the Faraday geometry as a function of QD composition (a) and size (b). Only the field component along the growth axis is shown. The solid gray lines show the box-model approximation based on the wave-function participation number.

Returning to the holes, one notes that for the amplitudes of the d-state admixtures used here, the magnitudes of the longitudinal fluctuations with and without the d-state admixture are very similar, which is, however, a coincidence. The dependence of the Overhauser field fluctuations on the assumed magnitude of d-shell admixture is shown in Fig. 3, where we present the results of calculations with the d-shell admixture magnitude for the nuclear species i set to $|\alpha_d^{(i)}|^2 = y|\alpha_d^{(i0)}|^2$, where $\alpha_d^{(i0)}$ are the values listed in Table I and used in the calculations presented above, and $0 < y < 1$. The dependence is nonmonotonic. In particular, $y \approx 0.5$ corresponds to mutual compensation of the p and d contributions to the coupling to indium ions, which dominate the overall effect due to their large nuclear momentum. As a result, the longitudinal fluctuations of the effective field are suppressed.

As discussed above, in the strongly confined self-assembled structure, the volume occupied by the wave function depends very weakly on the magnitude and orientation of the magnetic field. Therefore, one expects that the fluctuations of the Overhauser field will not depend on

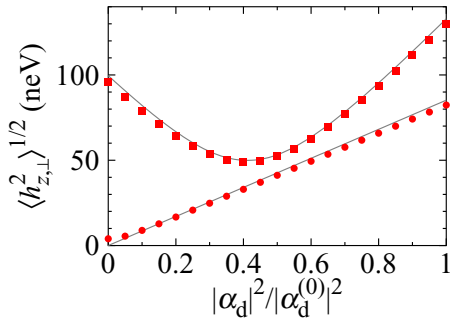

FIG. 3. The dependence of the root-mean-square average of the hyperfine field fluctuations on the magnitude of the d-shell admixture assumed in the calculations. Squares show the fluctuations of the field component along the growth (z) axis while circles represent the fluctuations of the transverse components (averaged over the in-plane directions). The admixtures for all the nuclei are scaled from 0 to the values given in Table I. The solid gray line shows the box-model approximation based on the wave-function participation number, given by Eq. (14).

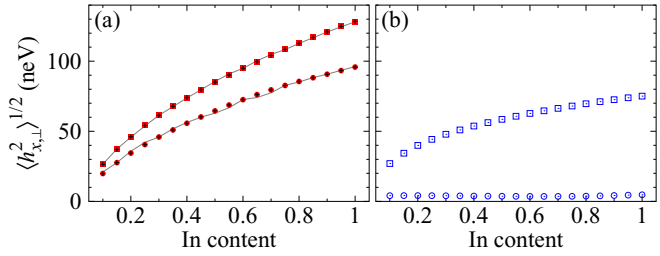

FIG. 4. The dependence of the root-mean-square average of the hyperfine field fluctuations as a function of QD composition in the Voigt geometry with (a) and without (b) atomic d-shell admixture. Circles and squares show the fluctuations along and perpendicular to the magnetic field, respectively, at $B = 8$ T. Crosses in (a) show the same results at $B = 1$ T. For comparison, the gray lines mark the results for the Faraday geometry.

the orientation of the magnetic field. Figure 4(a) shows the fluctuations of the Overhauser field in the Voigt geometry (magnetic field along x). The transverse component of the Overhauser field along the external magnetic field (the x component, shown by circles) is indeed the same as the transverse component in the Faraday geometry (shown by a gray line). The fluctuations perpendicular to the magnetic field (squares) now encompass the longitudinal (z) and the other transverse (y) component. Again, they perfectly agree with the corresponding average of these two components in the Faraday geometry (gray line). In addition, we performed computations in the Voigt geometry at $B = 1$ T, shown with crosses in Fig. 4(a). It is clear that the results do not depend on the field magnitude. In Fig. 4(b) we show analogous results from a model assuming no d-shell admixture. As expected, fluctuations perpendicular to the x direction are now much stronger than the ones along the x axis.

IV. DISCUSSION

The two main consequences of our calculations are the following. (1) The effects of band mixing on the magnitude of Overhauser field fluctuations experienced by hole spin in a self-assembled quantum dot are weak: for most of quantum dot sizes, shapes, and compositions one can use a simple single-envelope effective mass wave function to model the z component of the Overhauser field. The magnitude of transverse components of the Overhauser field due by band mixing is <5% of the longitudinal one. (2) Inclusion of effects of d-state admixture to the hole Bloch functions visibly affects the longitudinal fields, and it has an enormous effect on the transverse ones when one uses the amplitudes α_d of d-state admixtures similar to those inferred in [6] from isotope-resolved measurements of the longitudinal Overhauser fields caused by dynamically polarized nuclei. Most importantly, for $|\alpha_d|^2$ used in [6], and even for values up to 50% smaller, the Overhauser field experienced by the hole spin is almost isotropic.

Let us discuss the implications of the obtained results for hole-spin dephasing in Faraday and Voigt configurations. In Faraday configuration, the magnetic field B is along the z growth axis of the quantum dot, and the hole spin is initialized in superposition of up and down states along the z axis. We

assume that the hole-spin splitting $\Delta E = g_z \mu_B B$ (where g_z is the g factor of the hole for B along the z axis) is much larger than the transverse Overhauser fields, i.e., $B \gg 1$ mT assuming $g_z \approx 1$ and $\langle h_\perp^2 \rangle^{1/2} \leqslant 100$ neV. Dephasing of a freely precessing spin is then caused by averaging over a distribution of Overhauser fields along the z axis (longitudinal field in the terminology of this paper). The coherence in frame rotating with ΔE frequency is

$$|S_x(t) + iS_y(t)| \propto \exp[-(t/\tau_z)^2]$$

with $\tau_z = \sqrt{2}/\sigma_z$, where $\sigma_z = \langle h_z^2 \rangle^{1/2}$. For typical value of $\sigma_z \approx 100$ neV we have $T_2^* \approx 9$ ns.

In the Voigt configuration, with B along the x in-plane direction and $\Delta E = g_x \mu_B B \gg \sigma_z$ (where g_x is the in-plane hole g factor), we consider a hole spin initialized in eigenstate of S_z, a superposition of eigenstates of $\Delta E S_x$. Dephasing of this superposition is caused by averaging over contributions of h_x to the precession frequency, but also over corrections $(h_z^2 + h_y^2)/2\Delta E$ to this frequency caused by transverse fields [9,10]. In the Faraday configuration such corrections due to $h_\perp^2/2\Delta E$ were inefficient at dephasing compared to the linear coupling to h_z since $\langle h_\perp^2 \rangle^{1/2} < \langle h_z^2 \rangle^{1/2}$, and ΔE is larger by a factor of about 10 due to anisotropy of hole g factor. In the Voigt configuration the two mechanisms of dephasing can compete, albeit only at small magnetic fields.

Let us first consider the case of almost-isotropic hole hf interaction that we obtain using the d-state admixture parameters taken from [6]. In this case we have $\sigma_z \approx 150$ neV and $\sigma_\perp \equiv \langle h_\perp^2 \rangle^{1/2} \approx 100$ neV. Dephasing due to averaging over h_x is described by a Gaussian decay with time constant $\tau_x = \sqrt{2}/\sigma_\perp \approx 10$ ns. On the other hand, dephasing due to averaging over h_z and h_y fields is described by

$$|S_z(t) + iS_y(t)| \propto \frac{1}{[1 + (t/\tau_V)^2]^{1/2}},$$

with $\tau_V \approx \Delta E/\sigma_z^2$ (remember that $\sigma_y \approx \sigma_z$ is considered now). With $g_x \approx 0.1$, the half-decay time following from the above expression is $T_{1/2} = \sqrt{3}\tau_V \approx 300$ ns at $B = 1$ T, and only at fields <30 mT this time becomes shorter than $\tau_x \approx 10$ ns, and the coherence is then limited by fluctuations of h_z and h_y. At higher fields the decay is Gaussian with characteristic timescale given by τ_x.

On the other hand, in the limit of no d-state admixture, we have $\sigma_\perp \approx 5$ neV, and the Gaussian decay due to h_x fluctuations occurs in about 200 ns. The mechanism of dephasing due to second-order coupling to h_z (with h_y fluctuations being now negligible compared to those of h_z) leads then to the following form of the coherence decay [9,10]:

$$|S_z(t) + iS_y(t)| \propto \frac{1}{[1 + (t/\tau_V)^2]^{1/4}},$$

which results in half-decay time $T_{1/2} \approx 4\tau_V$. Assuming $g_x \approx 0.1$ and $\sigma_z \approx 150$ neV, for $B = 1$ T we obtain $T_{1/2} \approx 700$ ns, and we see that for $B \ll 0.3$ T the coherence decay should be dominated by this mechanism, and it should be possible to observe a characteristic $1/t^2$ tail of coherence decay when $t \ll 200$ ns. Finally, let us note that in [8] the measured values of rms of Overhauser fluctuations were $\sigma_z \approx 60$ neV and $\sigma_\perp \approx 0.5$ neV and in-plane g factor of the hole was $g_x \approx 0.05$ (actually 0.035 for one dot and 0.065 for another). These result in coherence half-decay time due to h_x fluctuations given by $T_{1/2} \approx 2$ μs at $B = 1$ T, which means that this mechanism will dominate over the Gaussian decay at fields already below a Tesla.

The results that we have obtained using α_d consistent with [6] are in clear disagreement with observations presented for the InGaAs quantum dot in [8], where a very small value of transverse Overhauser field (smaller by about an order of magnitude than the value that we predict for no d admixture, only due to heavy-light–hole mixing) was inferred from coherent population trapping experiment. Our results of small importance of band mixing and good applicability of the box-model approach to modeling of Overhauser field remove a few possible sources of inaccuracies that could have played a role in analysis of measurement results obtained in recent years. This strengthens the significance of disagreement in magnitudes of transverse Overhauser fields in InGaAs quantum dots inferred from these two very different experiments. Analysis in [6] is based on dynamic nuclear polarization (DNP) and measurement of isotope-resolved contributions to the *longitudinal* Overhauser shift. The isotope dependence of signs of these contributions was explained there by invoking a finite (and in fact quite substantial) admixture of d orbitals in heavy-hole states, but the value of transverse Overhauser field was not measured in that work. Such a measurement was performed in [8], in which a possible reason for disagreement with earlier experiments on dephasing of holes was suggested: the structure used in [8] was carefully designed to exhibit much less charge noise. It is now known that charge noise can contribute to (or even dominate) hole dephasing dynamics, due to electric-field dependence of hole g factor [8,14], so one has to be careful when attributing observed dephasing to hf interaction and using the measured coherence time to estimate $\langle h_{z,\perp}^2 \rangle^{1/2}$. This, however, has no bearing on the experiment and analysis of [6].

V. CONCLUSIONS

We have derived the eight-band $k \cdot p$ Hamiltonian for hyperfine interactions, including a proposed parametrization of Bloch functions consistent with the available experimental data. This offers a general formalism that allows one to include realistic multiband carrier wave functions, as obtained from $k \cdot p$ computations, in the calculation of hyperfine couplings. Using this formalism, we have studied the effect of fluctuations of the nuclear spin polarization on a hole in the ground state of an InGaAs QD for a range of realistic shapes and sizes, taking into account an admixture of atomic d orbitals to the valence band Bloch functions as well as band mixing. Our formalism can also be applied to problems in which accurate modeling of carrier states is crucial, e.g., when the hyperfine-related effects are to be combined with carrier-phonon couplings, compared with spin-orbit-induced effects or studied in coupled structures where tunneling plays a role.

One of the main results is the observation that in a wide range of dots shapes and sizes, the realistic description of carrier states, taking into account band mixing, envelope functions leakage into the barrier, etc., has little influence

on the root mean square of the Overhauser field fluctuations experienced by the spin of the heavy hole confined in the dot. These fluctuations can be well described using a "box" model of wave function, with effective number of nuclei strongly coupled to the hole being the only fitting parameter. Such a description was known to hold well for electrons, and it was widely used also for holes, but the justification of its quantitative accuracy was lacking until now in the latter case.

For the *transverse* (with respect to the growth axis) fluctuations of the Overhauser field, we have confirmed the relatively small effect of band mixing as compared to the d-state admixture, at least for the magnitude of this admixture inferred in [6] from isotope-resolved measurements of contributions to the *longitudinal* Overhauser field. The latter may lead to transverse fluctuations on the same order of magnitude as the longitudinal ones. The dependence of the longitudinal fluctuations on the amount of d admixture is strong and nonmonotonic. In the light of the fact that a large variability in the magnitude of both transverse and longitudinal fluctuations was reported in experiments, these results suggest the need for careful examination of dependence of the magnitude of the d-state admixtures to wave functions localized close to cation and anion cores (and also the spatial extent of the relevant d orbitals, as it has a large influence on the value of hf interaction), as a function of indium content (and possibly strain) in InGaAs/GaAs QDs.

ACKNOWLEDGMENTS

This work was supported by the Polish National Science Centre under Grant No. 2014/13/B/ST3/04603. Calculations have been carried out using resources provided by Wroclaw Centre for Networking and Supercomputing [54], Grant No. 203. We would like to thank P. Bogusławski for interesting discussion of the origins of d-state admixtures in valence band states.

APPENDIX: DERIVATION OF THE MATRIX ELEMENTS OF THE HYPERFINE COUPLING

The main purpose of this Appendix is to rigorously derive the matrix elements of the short-range multiband hyperfine Hamiltonian as given in Eqs. (12a)–(12f). In the following, we will focus on one selected nucleus located at $\boldsymbol{R}_0$ and the index α will be suppressed. The three contributions to $\boldsymbol{A}$ in Eq. (2) will be denoted, respectively, as $\boldsymbol{A}_\mathrm{c}$ (the contact interaction), $\boldsymbol{A}_\mathrm{o}$ (the orbital part of the dipole interaction), and $\boldsymbol{A}_\mathrm{s}$ (the spin part of the dipole interaction).

For the general calculations to be performed, it is convenient to use spherical tensor representation of various vectorial and tensorial quantities that appear in the derivations. Before we proceed to the technical derivations, let us note that this is a natural language for discussing the hyperfine spin-flip selection rules. The essential part of the hyperfine Hamiltonian in Eq. (1) is

$$\boldsymbol{A}(\boldsymbol{r}-\boldsymbol{R}_0)\cdot\boldsymbol{I} = -\sqrt{3}\sum_{q_1 q_2}\langle 1,1;q_1,q_2|1,1;0,0\rangle \times A^{(1)}_{q_1}(\boldsymbol{r}-\boldsymbol{R}_0)I^{(1)}_{q_2}, \tag{A1}$$

where the upper index denotes the rank of the tensor and, at the same time, distinguishes the spherical tensor components from the Cartesian ones, $\langle j_1, j_2; m_1, m_2|j_1, j_2; j, m\rangle$ is the Clebsch-Gordan coefficient, and the spherical components of any vector $\boldsymbol{V}$ are defined in the standard way

$$V^{(1)}_0 = V_z, \quad V^{(1)}_{\pm 1} = \frac{\mp V_x - iV_y}{\sqrt{2}} = \mp\frac{1}{\sqrt{2}}V_\pm.$$

The range of q_1, q_2 is not given explicitly upon assumption that ill-defined Clebsch-Gordan coefficients are 0. Explicitly, $\boldsymbol{A}\cdot\boldsymbol{I} = A^{(1)}_0 J^{(1)}_0 - A^{(1)}_{-1}J^{(1)}_{+1} - A^{(1)}_{+1}J^{(1)}_{-1} = A_z J_z + (A_- J_+ + A_+ J_-)/2$. The $q=0$ term thus corresponds to the Ising coupling. The $q=\pm 1$ terms account for spin flip-flop processes, in which the carrier exchanges its spin with the nucleus. In the simplest picture of hole states with definite angular momentum and composed exclusively of p orbitals, the contact part $\boldsymbol{A}_\mathrm{c}$ does not contribute to valence band hyperfine coupling due to vanishing p-type wave functions at the position of the nucleus. The other two terms can only contribute to diagonal terms since the vector operator $\boldsymbol{A}$ cannot couple states with $m_j = \pm\frac{3}{2}$, that is, differing by $|\Delta m_j| = 3$. Hence, in this single-band approximation, only the Ising term appears for heavy holes. However, symmetry reduction in a nanostructure modifies this simple picture by mixing the states belonging to different representations of angular momentum due to band mixing as well as by admixing d-shell atomic orbitals to valence band Bloch functions.

For the derivations we note that, by comparing Eq. (8) with Eq. (11), the Hamiltonian blocks $\tilde{H}_{b'b}$ contain grouped elements $3\boldsymbol{A}_{\lambda'\lambda}\cdot\boldsymbol{I}/(\hbar a^{(\lambda')*}a^{\lambda})$. We will now derive these elements for each of the three contributions to the hyperfine Hamiltonian.

1. Contact part

The contact part, i.e., the first term in Eq. (2), has contributions only from the conduction bands (s-type atomic orbitals, $l=m=0$). One has $u_{\mathrm{e}\uparrow}(\boldsymbol{r},\uparrow) = u_{\mathrm{e}\downarrow}(\boldsymbol{r},\downarrow) = \sqrt{v}a^{(\mathrm{cb})}_\alpha S(r)/\sqrt{4\pi}$, $u_{\mathrm{e}\uparrow}(\boldsymbol{r},\downarrow) = u_{\mathrm{e}\downarrow}(\boldsymbol{r},\uparrow) = 0$, where $S_\alpha(r) = 4\xi_s^3/a_\mathrm{B}^3$ is the radial part of the atomic s-type wave function for a given ion. Hence, using Eq. (7) transformed to spherical tensor components, the contact interaction has the matrix elements

$$A^{(1)}_{\mathrm{c},q;\lambda'\lambda} = \frac{2\xi_s^3}{3\hbar}\left(S^{(1)}_q\right)_{s_{\lambda'}s_\lambda},$$

where s_λ is the spin projection of the electrons in band λ. From the Wigner-Eckart theorem one finds

$$\left(S^{(1)}_q\right)_{s's} = \frac{\sqrt{3}\hbar}{2}\left\langle\frac{1}{2},1;s,q\middle|\frac{1}{2},1;\frac{1}{2},s'\right\rangle.$$

Hence, the nonzero matrix elements of the spherical components of the spin operator are

$$\left(S^{(1)}_0\right)_{\uparrow\uparrow} = -\left(S^{(1)}_0\right)_{\downarrow\downarrow} = \frac{\hbar}{2},$$
$$-\left(S^{(1)}_{+1}\right)_{\uparrow\downarrow} = \left(S^{(1)}_{-1}\right)_{\downarrow\uparrow} = \frac{\hbar}{\sqrt{2}}.$$

Collecting the elements of the 6c6c block and converting to Cartesian components one finds $A_{\mathrm{c},i} = \xi_s^3 |a_\alpha^{(\mathrm{cb})}|^2 \sigma_i/3$, hence, $\tilde{H}_{6\mathrm{c}6\mathrm{c}} = 3\boldsymbol{A}_c \cdot \boldsymbol{I}/(\hbar |a_\alpha^{(\mathrm{cb})}|^2) = \boldsymbol{\sigma} \cdot \boldsymbol{I}/\hbar$, which proves Eq. (12a).

2. Orbital term of the dipole part

For the local term of $\boldsymbol{A}_o$ [the second term in Eq. (2)], one substitutes the decomposition in Eq. (9) into Eq. (6). The hydrogenlike orbitals $f_{lm}(\boldsymbol{r})$ building the Bloch function according to Eq. (9) are decomposed into their radial parts $\mathcal{R}(r)$ and angular parts described by spherical harmonics $Y_{l,m}(\Omega)$. Taking into account that the components of the angular momentum operator are diagonal in spin s and in the total angular momentum l, one gets

$$\frac{A^{(1)}_{\mathrm{o},q;\lambda'\lambda}}{\left(a_\alpha^{(\lambda')*} a_\alpha^{\lambda}\right)} = \xi_s^3 \sum_{lmm's} M_{ll} c_{lm'}^{(\lambda' s)*} c_{lm}^{(\lambda s)} \langle lm'|L_q^{(1)}|lm\rangle,$$

where

$$M_{l'l} = \frac{a_\mathrm{B}^3}{4\xi_s^3} \int dr\, r^2 \mathcal{R}_{l'}^*(\boldsymbol{r}) \frac{1}{r^3} \mathcal{R}_l(\boldsymbol{r}).$$

Following [6] we denote $M_{11} \equiv M_\mathrm{p} M_{22} \equiv M_\mathrm{d}$, $M_{02} = M_{20} \equiv M_\mathrm{sd}$. The matrix elements $\langle lm'|L_q^{(1)}|lm\rangle$ can be trivially calculated by elementary methods. However, a more compact and uniform result is obtained via Wigner-Eckart theorem

$$\langle lm'|L_q^{(1)}|lm\rangle = \frac{\langle l, 1; m, q | l, 1; l, m'\rangle}{\sqrt{2l+1}} \langle l||L^{(1)}||l\rangle.$$

The reduced matrix element is found by inspection of the component $q = 0$, $m = m'$ where $\langle l, 1; m, 0|l, 1; lm'\rangle = m/\sqrt{l(l+1)}$ and obviously $\langle lm|L_0^{(1)}|lm\rangle = m$, hence, $\langle l||L^{(1)}||l\rangle = \sqrt{l(l+1)(2l+1)}$. Hence, the final formula is

$$\frac{\langle \lambda'|\mathcal{A}^{(1)}_{\mathrm{o,SR},q}|\lambda\rangle}{\left(\hbar a_\alpha^{(\lambda')*} a_\alpha^{\lambda}\right)} = \xi_s^3 \sum_{lmm's} M_{ll} c_{lm'}^{(\lambda' s)*} c_{lm}^{(\lambda s)} \times \sqrt{l(l+1)} \langle l, 1; m, q | l, 1; l, m'\rangle. \quad \text{(A2)}$$

We note that this matrix element is diagonal in l and vanishes for $l = 0$, hence, nonzero matrix elements appear only within the valence band. Moreover, for the heavy-hole (hh) bands, in the simple single-band approximation, the Bloch functions are spin eigenstates with opposite spin orientation. Since the orbital contribution is spin diagonal, in the single-band, purely p-wave model of the hh band, this term yields only a diagonal (Ising) coupling. This coupling is affected by band mixing only in the second order since neither the spin-down nor the $m' = 0, -1$ spin-up admixture couple to the leading-order ($m = 1$ spin-up) component of the nominally spin-up hh state via the $q = 0$ tensor component (due to spin conservation and $m + q = m'$ selection rule, respectively). A d-shell admixture introduces a $l = 2$, $m' = -1$ spin-up correction to the spin-up hh state (see the explicit compositions of the Bloch states in [6]). This is not coupled to the leading-order ($l = 1$) component of this state but couples to the same ($l = 2$, $m = -1$) admixture, leading to a correction to the Overhauser field in the quadratic order in α_d.

In addition, with band mixing, the nominally $+\frac{3}{2}$ (spin-up) hh state ($m' = 1$) may attain an admixture of the spin-down light hole state with $m' = 0$. According to Eq. (A2), this admixture is coupled to the dominating component of the $-\frac{3}{2}$ (spin-down) hh state ($m = -1$) via the $q = 1$ component of the hyperfine coupling, thus leading to the appearance of spin flip-flop terms in the Hamiltonian. The d-wave admixture to hh Bloch functions is spin conserving, hence, it can only lead to spin flip flops in combination with band mixing.

3. Spin term of the dipole part

The third term in Eq. (2) can be written in terms of Cartesian components as

$$A_{\mathrm{s},i} = \sum_j T_{ij} S_j/\hbar,$$

where

$$T_{ij} = \frac{a_\mathrm{B}^3}{4} \frac{3x_i x_j - r^2 \delta_{ij}}{r^5}$$

is a traceless, symmetric, second-order Cartesian tensor, hence, its components form a second-order spherical tensor. The spherical components of $\boldsymbol{A}_\mathrm{s}$ are

$$A^{(1)}_{\mathrm{s},q} = -\sqrt{15} \sum_{q_1,q_2} \langle 2, 1; q_1, q_2 | 2, 1; 1, q\rangle T^{(2)}_{q_1} S^{(1)}_{q_2},$$

where the spherical components of $T^{(2)}$ are constructed from the first-order position tensor $r^{(1)}$ according to the tensor multiplication rule

$$T^{(2)}_q = \frac{a_\mathrm{B}^3}{4r^5} \sum_{q_1,q_2} \langle 1, 1; q_1, q_2 | 1, 1; 2, q\rangle r^{(1)}_{q_1} r^{(1)}_{q_2} = \frac{a_\mathrm{B}^3}{4r^3} \sqrt{\frac{8\pi}{15}} Y_{2,q}(\hat{\boldsymbol{r}}),$$

and the overall factor has been determined by inspection.

The matrix element of $T_q^{(2)}$ between two hydrogenlike orbitals is

$$\int d^3 r\, f^*_{l'm'}(\boldsymbol{r}) T^{(2)}_q f_{lm}(\boldsymbol{r}) = \sqrt{\frac{8\pi}{15}} M_{l'l} G^{m'qm}_{l'2l}, \quad \text{(A3)}$$

where $G^{mm'm''}_{ll'l''}$ are Gaunt coefficients,

$$G^{mm'm''}_{ll'l''} = \int d\Omega\, Y^*_{l,m}(\Omega) Y_{l',m'}(\Omega) Y_{l''m''}(\Omega) = (-1)^m \sqrt{\frac{(2l+1)(2l'+1)(2l''+1)}{4\pi}} \times \begin{pmatrix} l & l' & l'' \\ 0 & 0 & 0 \end{pmatrix} \begin{pmatrix} l & l' & l'' \\ m & m' & m'' \end{pmatrix},$$

and $\left(\begin{smallmatrix} l & l' & l'' \\ m & m' & m'' \end{smallmatrix}\right)$ are Wigner 3-j symbols. From the parity rule on the Gaunt coefficients $l + l' + l''$, even, and the triangle rule $|l - l''| \leqslant l' \leqslant l + l''$, the only nonzero contributions in Eq. (A3) are those with $(l, l') = (0, 2), (2, 0), (1, 1), (2, 2)$. Hence, nonzero matrix elements appear within the valence band, and between the valence and conduction bands.

Upon substituting the result from Eq. (A3), along with the decomposition in Eq. (9), to Eq. (7) one gets

$$\frac{\langle\lambda'|\mathcal{A}^{(1)}_{\mathrm{s,SR},q}|\lambda\rangle}{(\hbar a^{(\lambda')*}_{\alpha} a^{\lambda}_{\alpha})} = -\sqrt{8\pi}\xi_s^3 \sum_{lms}\sum_{l'm's'} M_{l'l} \times \sum_{q_1,q_2}\langle 2,1;q_1,q_2|2,1;1,q\rangle \times G^{m'q_1m}_{l'2l} c^{(\lambda's')*}_{l'm'} c^{(\lambda s)}_{lm} \left(S^{(1)}_{q_2}\right)_{s's}. \quad \text{(A4)}$$

The structure of this term is much more complicated than that of the orbital contribution since the present term is not diagonal in l and s. The Clebsch-Gordan coefficient requires $q_1 + q_2 = q$, while the Gaunt and $M_{ll'}$ coefficients impose the selection rules $m' = m + q_1$ and $(l', l) = (1, 1)$, (2,2), (0,2), or (2,0).

We start with analyzing the corrections to the heavy-hole Overhauser field Ising term $q = 0$. The three nonvanishing decompositions are now $q_1 = \pm 1$, $q_2 = \mp 1$ and $q_1 = 0$, $q_2 = 0$. The contribution $(l', l) = (1, 1)$ yields the leading-order (hh-hh) part of the Ising coupling ($q_1 = q_2 = 0$) as well as coupling between components that differ by spin-orbital angular momentum flip flop (e.g., $m' = 1$, $s' = \uparrow$ to $m = 0$, $s' = \downarrow$). For the p-wave component, the latter is only possible for light-hole states, hence, the resulting correction must rely on light-hole admixtures to *both* hh states and is therefore quadratic in band-mixing amplitudes. The contribution $(l', l) = (2, 2)$ clearly involves d-wave contributions to both states and is therefore always quadratic in the d-wave amplitude α_d. It contains the contribution from the leading-order component of the hh state as well as the spin-orbital flip-flop couplings between light-hole components of the hh state, which are, additionally, quadratic in band mixing. The term with $(l', l) = (0, 2)$ couples the conduction band (cb) admixture to the d-wave component of the leading-order contribution of the hh state. It is, therefore, linear in α_d but one should remember that the cb admixture is very small.

In addition, band mixing and d-wave contributions to Bloch functions generate terms with $q = \pm 1$ in the Hamiltonian, that is, flip-flop couplings between the hh states and the nuclei. For instance, for $(l', l) = (1, 1)$, there is a contribution from the $q_1 = 0$, $q_2 = 1$ term, coupling the leading-order contribution to the hh state ($m = 1$, spin up) with a light-hole admixture to the other hh state ($m = 1$, spin down), which is linear in band mixing and therefore should be much larger than the band-mixing corrections to the Overhauser term. Another such coupling appears for $(l', l) = (2, 2)$ and $q_1 = 2$, $q_2 = -1$. This one couples the $m = 1$ spin-down and $m = -1$ spin-up components, that is, the d-wave components of the leading contribution to the two opposite hh states.

Equation (A2) together with Eq. (A4), upon converting to Cartesian components and explicit evaluation, yield the matrix representation used in Eqs. (12b)–(12f).

[1] B. D. Gerardot, D. Brunner, P. A. Dalgarno, P. Ohberg, S. Seidl, M. Kroner, K. Karrai, N. G. Stoltz, P. M. Petroff, and R. J. Warburton, Optical pumping of a single hole spin in a quantum dot, Nature (London) **451**, 441 (2008).

[2] D. Brunner, B. D. Gerardot, P. A. Dalgarno, G. Wost, K. Karrai, N. G. Stoltz, P. M. Petroff, and R. J. Warburton, Optical pumping of a single hole spin in a quantum dot, Science **325**, 70 (2009).

[3] B. Eble, C. Testelin, P. Desfonds, F. Bernardot, A. Balocchi, T. Amand, A. Miard, A. Lemaître, X. Marie, and M. Chamarro, Hole-Nuclear Spin Interaction in Quantum Dots, Phys. Rev. Lett. **102**, 146601 (2009).

[4] P. Fallahi, S. T. Yilmaz, and A. Imamoğlu, Measurement of A Heavy-Hole Hyperfine Interaction in Ingaas Quantum Dots Using Resonance Fluorescence, Phys. Rev. Lett. **105**, 257402 (2010).

[5] E. A. Chekhovich, A. B. Krysa, M. S. Skolnick, and A. I. Tartakovskii, Direct Measurement of the Hole-Nuclear Spin Interaction in Single InP/GaInP Quantum Dots Using Photoluminescence Spectroscopy, Phys. Rev. Lett. **106**, 027402 (2011).

[6] E. A. Chekhovich, M. M. Glazov, A. B. Krysa, M. Hopkinson, P. Senellart, A. Lemaître, M. S. Skolnick, and A. I. Tartakovskii, Element-sensitive measurement of the hole-nuclear spin interaction in quantum dots, Nat. Phys. **9**, 74 (2012).

[7] S. G. Carter, S. E. Economou, A. Greilich, E. Barnes, T. Sweeney, A. S. Bracker, and D. Gammon, Strong hyperfine-induced modulation of an optically driven hole spin in an inas quantum dot, Phys. Rev. B **89**, 075316 (2014).

[8] J. H. Prechtel, A. V. Kuhlmann, J. Houel, A. Ludwig, S. R. Valentin, A. D.Wieck, and R. J.Warburton, Decoupling a hole spin qubit from the nuclear spins, Nat. Mater. **15**, 981 (2016).

[9] J. Fischer, W. A. Coish, D. V. Bulaev, and D. Loss, Spin decoherence of a heavy hole coupled to nuclear spins in a quantum dot, Phys. Rev. B **78**, 155329 (2008).

[10] C. Testelin, F. Bernardot, B. Eble, and M. Chamarro, Hole-spin dephasing time associated with hyperfine interaction in quantum dots, Phys. Rev. B **79**, 195440 (2009).

[11] K. De Greve, P. L. McMahon, D. Press, T. D. Ladd, D. Bisping, C. Schneider, M. Kamp, L. Worschech, S. Höfling, A. Forchel, and Y. Yamamoto, Ultrafast coherent control and suppressed nuclear feedback of a single quantum dot hole qubit, Nat. Phys. **7**, 872 (2011).

[12] A. Greilich, S. G. Carter, D. Kim, A. S. Bracker, and D. Gammon, Optical control of one and two hole spins in interacting quantum dots, Nat. Photonics **5**, 702 (2011).

[13] A. Delteil, Z. Sun, W.-B. Gao, E. Togan, S. Faelt, and A. Imamoglu, Generation of heralded entanglement between distant hole spins, Nat. Phys. **12**, 218 (2016).

[14] L. Huthmacher, R. Stockill, E. Clarke, M. Hugues, C. Le Gall, and M. Atatüre, Coherence of a dynamically decoupled quantum-dot hole spin, Phys. Rev. B **97**, 241413(R) (2018).

[15] J. Schliemann, A. Khaetskii, and D. Loss, Electron spin dynamics in quantum dots and related nanostructures due to hyperfine interaction with nuclei, J. Phys.: Condens. Matter **15**, R1809 (2003).

[16] W. A. Coish and J. Baugh, Nuclear spins in nanostructures, Phys. Status Solidi B **246**, 2203 (2009).

[17] Ł. Cywiński, Dephasing of electron spin qubits due to their interaction with nuclei in quantum dots, Acta Phys. Pol. A **119**, 576 (2011).

[18] B. Urbaszek, X. Marie, T. Amand, O. Krebs, P. Voisin, P. Maletinsky, A. Högele, and A. Imamoğlu, Nuclear spin physics in quantum dots: An optical investigation, Rev. Mod. Phys. **85**, 79 (2013).

[19] E. A. Chekhovich, M. N. Makhonin, A. I. Tartakovskii, A. Yacoby, H. Bluhm, K. C. Nowack, and L. M. K. Vandersypen, Nuclear spin effects in semiconductor quantum dots, Nat. Mater. **12**, 494 (2013).

[20] M. M. Glazov, *Electron and Nuclear Spin Dynamics in Semiconductor Nanostructures* (Oxford University Press, Oxford, 2018), p. 283.

[21] K. De Greve, D. Press, P. L. McMahon, and Y. Yamamoto, Ultrafast optical control of individual quantum dot spin qubits, Rep. Prog. Phys. **76**, 092501 (2013).

[22] R. J. Warburton, Single spins in self-assembled quantum dots, Nat. Mater. **12**, 483 (2013).

[23] M. I. D'yakonov and V. I. Perel', Dynamic self-polarization of nuclei in solids, Pis'ma v ZhETF **16**, 563 (1972) [JETP Lett. **10**, 398 (1972)].

[24] E. I. Gryncharova and V. I. Perel', Relaxation of nuclear spins interacting with holes in semiconductors, Fiz. Tekh. Poluprovodn. **11**, 1697 (1977) [Sov. Phys.–Semicond. **11**, 997 (1977)].

[25] Y. Obata, Nuclear magnetic relaxation in transition metals, J. Phys. Soc. Jpn. **18**, 1020 (1963).

[26] E. B. Hale and R. L. Mieher, Calculation of anisotropic hyperfine constants for lattice nuclei near a shallow donor, Phys. Rev. B **3**, 1955 (1971).

[27] J. G. Díaz and G. W. Bryant, Electronic and optical fine structure of GaAs nanocrystals: The role of d orbitals in a tight-binding approach, Phys. Rev. B **73**, 075329 (2006).

[28] D. J. Chadi, Angular momentum decomposition of Bloch functions in group IV and zincblende crystals, Solid State Commun. **20**, 361 (1976).

[29] C. Persson and A. Zunger, *s-d* coupling in zinc-blende semiconductors, Phys. Rev. B **68**, 073205 (2003).

[30] P. Boguslawski and I. Gorczyca, Atomic-orbital interpretation of electronic structure of iii-v semiconductors: Gaas versus alas, Semicond. Sci. Technol. **9**, 2169 (1994).

[31] E. A. Chekhovich, K. V. Kavokin, J. Puebla, A. B. Krysa, M. Hopkinson, A. D. Andreev, A. M. Sanchez, R. Beanland, M. S. Skolnick, and A. I. Tartakovskii, Structural analysis of strained quantum dots using nuclear magnetic resonance, Nat. Nanotechnol. **7**, 646 (2012).

[32] G. Bester and A. Zunger, Cylindrically shaped zinc-blende semiconductor quantum dots do not have cylindrical symmetry: Atomistic symmetry, atomic relaxation, and piezoelectric effects, Phys. Rev. B **71**, 045318 (2005).

[33] H. Wei, G.-C. Guo, and L. He, Tuning of the hole spin relaxation time in single self-assembled $In_{1-x}Ga_xAs/GaAs$ quantum dots by electric field, J. Appl. Phys. **116**, 204304 (2014).

[34] M. Zieliński, Including strain in atomistic tight-binding Hamiltonians: An application to self-assembled InAs/GaAs and InAs/InP quantum dots, Phys. Rev. B **86**, 115424 (2012).

[35] M. Ehrhardt and T. Koprucki, *Multi-Band Effective Mass Approximations* (Springer, Cham, 2014).

[36] K. Gawarecki, Spin-orbit coupling and magnetic-field dependence of carrier states in a self-assembled quantum dot, Phys. Rev. B **97**, 235408 (2018).

[37] A. Schliwa, M. Winkelnkemper, and D. Bimberg, Impact of size, shape, and composition on piezoelectric effects and electronic properties of InGaAs, Phys. Rev. B **76**, 205324 (2007).

[38] K. Gawarecki and P. Machnikowski, Phonon-assisted relaxation between hole states in quantum dot molecules, Phys. Rev. B **85**, 041305(R) (2012).

[39] V. Jovanov, T. Eissfeller, S. Kapfinger, E. C. Clark, F. Klotz, M. Bichler, J. G. Keizer, P. M. Koenraad, M. S. Brandt, G. Abstreiter, and J. J. Finley, Highly nonlinear excitonic Zeeman spin splitting in composition-engineered artificial atoms, Phys. Rev. B **85**, 165433 (2012).

[40] T. Andlauer and P. Vogl, Electrically controllable g tensors in quantum dot molecules, Phys. Rev. B **79**, 045307 (2009).

[41] R. Winkler, *Spin-Orbit Coupling Effects in Two-Dimensional Electron and Hole Systems*, Springer Tracts in Modern Physics, Vol. 191 (Springer, Berlin, 2003).

[42] A. Mielnik-Pyszczorski, K. Gawarecki, M. Gawełczyk, and P. Machnikowski, Dominant role of the shear strain induced admixture in spin-flip processes in self-assembled quantum dots, Phys. Rev. B **97**, 245313 (2018).

[43] M. Gawełczyk, M. Krzykowski, K. Gawarecki, and P. Machnikowski, Controllable electron spin dephasing due to phonon state distinguishability in a coupled quantum dot system, Phys. Rev. B **98**, 075403 (2018).

[44] A. Musiał, P. Kaczmarkiewicz, G. Sęk, P. Podemski, P. Machnikowski, J. Misiewicz, S. Hein, S. Höfling, and A. Forchel, Carrier trapping and luminescence polarization in quantum dashes, Phys. Rev. B **85**, 035314 (2012).

[45] E. Clementi and D. L. Raimondi, Atomic Screening Constants from SCF Functions, J. Chem. Phys. **38**, 2686 (1963).

[46] E. Clementi, Atomic Screening Constants from SCF Functions. II. Atoms with 37 to 86 Electrons, J. Chem. Phys. **47**, 1300 (1967).

[47] L. C. Lew Yan Voon and M. Willatzen, *The $k \cdot p$ Method* (Springer, Berlin, 2009).

[48] C. Pryor, J. Kim, L. W. Wang, A. J. Williamson, and A. Zunger, Comparison of two methods for describing the strain profiles in quantum dots, J. Appl. Phys. **83**, 2548 (1998).

[49] G. Bester, A. Zunger, X. Wu, and D. Vanderbilt, Effects of linear and nonlinear piezoelectricity on the electronic properties of InAs/GaAs quantum dots, Phys. Rev. B **74**, 081305(R) (2006).

[50] T. Andlauer, R. Morschl, and P. Vogl, Gauge-invariant discretization in multiband envelope function theory and g factors in nanowire dots, Phys. Rev. B **78**, 075317 (2008).

[51] R. Benchamekh, F. Raouafi, J. Even, F. Ben Cheikh Larbi, P. Voisin, and J.-M. Jancu, Microscopic electronic wave function and interactions between quasiparticles in empirical tight-binding theory, Phys. Rev. B **91**, 045118 (2015).

[52] E. A. Chekhovich, A. Ulhaq, E. Zallo, F. Ding, O. G. Schmidt, and M. S. Skolnick, Measurement of the spin temperature of optically cooled nuclei and gaas hyperfine constants in gaas/algaas quantum dots, Nat. Mater. **16**, 982 (2017).

[53] B. Kramer and A. MacKinnon, Localization: theory and experiment, Rep. Prog. Phys. **56**, 1469 (1993).

[54] http://wcss.pl.